Macromolecules

pubs.acs.org/Macromolecules Article

Short-Time Dynamics of PDMS-*g*-PDMS Bottlebrush Polymer Melts Investigated by Quasi-Elastic Neutron Scattering

Karin J. Bichler,* Bruno Jakobi, Victoria García Sakai, Alice Klapproth, Richard A. Mole, and Gerald J. Schneider*

Cite This: *Macromolecules* 2020, 53, 9553–9562 Read Online

ACCESS | Metrics & More | Article Recommendations | Supporting Information

ABSTRACT: We have studied the short-time dynamical behavior of polydimethylsiloxane (PDMS) bottlebrush polymers, PDMS-*g*-PDMS. The samples have similar backbone lengths but different side-chain lengths, resulting in a shape transition. Quasi-elastic neutron scattering was used to observe the dynamical changes inherent to these structural changes. The combination of data from three spectrometers enabled to follow the dynamics over broad frequency and temperature ranges, which included segmental relaxations and more localized motions. The latter, identified as the methyl group rotation, is described by a threefold jump model and shows higher activation energies compared to linear PDMS. The segmental relaxation times, τ_s, decrease with increasing molecular weight of the side chains but increase with momentum transfer, Q, following a power law, which suggests a non-Gaussian behavior for bottlebrush polymers.

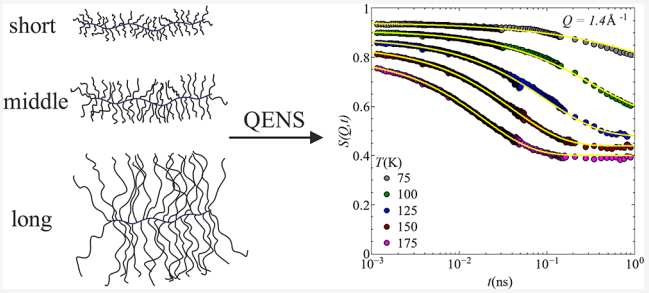

INTRODUCTION

Bottlebrush polymers, i.e., linear side chains covalently bonded to a linear backbone, have received great interest in recent times. These architectural modifications cause shape changes, such as from spherical into elongated objects, simply by varying the size ratio of backbone to side-chain length.[1−7] Inherent with the bottlebrush architecture are extraordinary properties, such as super softness or low viscosity. These properties are desirable in the development of new materials. Novel composites that take advantage of shell-only particles or surface modifications can be envisioned.[3,8,9] The resulting macroscopic behavior is governed by microscopic relaxation processes. However, only little is known about the dynamics of bottlebrush polymer melts. For polymers with a linear architecture or very short side chains, the relaxation spectra are dominated by the backbone.[10] If side chains exceed a certain length, rheology can detect the emergence of new processes.[11] In bottlebrushes, the shape transition from elongated into spherical shapes may change the molecular dynamics of the system. We have investigated the short-time dynamics of polydimethylsiloxane (PDMS)-based bottlebrush polymers, PDMS-*g*-PDMS, for the first time, by quasi-elastic neutron scattering (QENS). In the current study, three different samples were considered, with similar backbones but different lengths of the side chain. The existence of the shape transition in these samples has been confirmed by small-angle neutron scattering (SANS) experiments.[12]

Dynamical processes in polymers evolve over several orders of magnitude in time. To cover such a broad time range with QENS, a combination of three different spectrometers was used in this study, covering a time range of t = 1 ps to t = 1 ns. By analyzing the dependence of the incoherent intermediate scattering function, $S(Q,t) := S_{inc}(Q,t)$, on the time, t, and the momentum transfer, Q, we obtain information about the geometrical confinement of localized motions as well as the relaxation times of the individual processes.

EXPERIMENTAL SECTION

QENS measures the dynamic structure factor which comprises coherent and incoherent parts resulting from the scattering event such that $S(Q,\omega) = S_{coh}(Q,\omega) + S_{inc}(Q,\omega)$. The samples studied here are protonated PDMS-*g*-PDMS bottlebrush polymers, and as such, because of the large incoherent scattering cross section of hydrogen, $\sigma_{inc} = 80.26 \times 10^{-24}$ cm^2, the measured dynamical structure factor is dominated by the incoherent part. Therefore, in our case, $S(Q,\omega) = S_{inc}(Q,\omega)$.

The measured intensity, $S_{exp}(Q,\omega)$, is a convolution of the pure sample scattering, $S_{inc}(Q,\omega)$, with the instrument-specific resolution, $R(Q,\omega)$, i.e., $S_{exp}(Q,\omega) = S_{inc}(Q,\omega) \otimes R(Q,\omega)$. The resolution, which represents the longest timescale that can be probed by the instrument, is a fundamental property of the spectrometer used to measure the signal. As the temperature is changed, it is not uncommon for a signal

Received: August 9, 2020
Revised: September 28, 2020
Published: October 20, 2020

https://dx.doi.org/10.1021/acs.macromol.0c01846
Macromolecules 2020, 53, 9553–9562

to shift from the dynamic range of one instrument to another. In reciprocal and energy space, the resolution is convoluted with the sample scattering, while if one performs the time Fourier transformation of the data to get the intermediate scattering function, $S_{inc}(Q,t)$, the convolution is a simple multiplication.

$$S_{exp}(Q, t) = S_{inc}(Q, t)\cdot R(Q, t) \quad (1)$$

Doing this implies that it becomes easier to account for the resolution and thus compare the dynamic structure factor across a number of instruments.

$$S_{inc}(Q, t) = \frac{\int S_{exp}(Q, \omega)\exp(i\omega t)\mathrm{d}\omega}{\int R(Q, \omega)\exp(i\omega t)\mathrm{d}\omega} \quad (2)$$

In order to cover a broad dynamical range, we have used a combination of three different QENS instruments, the time-of-flight spectrometer Pelican[13] at ANSTO, the time-of-flight backscattering instrument IRIS[14] at ISIS, and the backscattering instrument EMU[15] at ANSTO. Each of them has a different energy transfer and energy resolution, resulting in different time ranges. The technical specifications of the instruments are summarized in Table 1.

Table 1. Specifications of the Different QENS Instruments Used for Our Experiment

location	instrument	energy resolution (μeV)	energy range (meV)	Q-range (Å^{-1})
ANSTO	EMU	1.1	−0.028 to 0.028	0.4−1.8
ISIS	IRIS	17.5	−0.55 to 0.57	0.6−1.6
ANSTO	Pelican	65	−19.99 to 2.59	0.2−1.8

All measurements were conducted in a temperature range of T = 75 K to T = 300 K, accompanied with a measurement of the instrument resolution at low temperature, specifically at T = 1.5 K on EMU and Pelican and at T < 10 K on IRIS. For the temperature control, a closed-cycle cryostat with a secondary helium circulation loop, controlled by a needle valve (EMU and Pelican), and a closed-cycle refrigerator (IRIS) were used. This allowed a base temperature of T < 10 K.

For the normalization against detector efficiency, standard vanadium calibration data were used for each instrument. The samples were loaded into aluminum cans with aluminum screws provided by ANSTO, and all measurements were carried out with these same cans, to ensure consistency over the three instruments. The sample gap was chosen to be 0.1 mm, which ensures 90% transmission and minimizes multiple scattering. For all experiments, the program MANTID[16] was used for data reduction, employing existing routines specific for each of the three spectrometers.

Backscattering Instrument—EMU. EMU is a neutron backscattering instrument located at ANSTO, Sydney, Australia.[15] Neutrons with a wavelength of λ = 6.28 Å are selected *via* a pyrolytic graphite crystal premonochromator *via* their (002) Bragg reflection. The continuous beam is split by a background chopper into several bunches, i.e., the neutron beam is pulsed to reduce background scattering. The following graphite chopper, that is, a disc chopper with graphite elements located at the periphery, deflects the neutrons, in its closed position, to the Doppler drive. The Doppler drive oscillates with a maximum velocity of v_{max} = 4.7 m/s and shifts the neutrons in energy, creating an energy distribution of $(E_i \pm \delta E)(t)$. The Doppler-shifted neutrons pass the graphite chopper in the open position and scatter at the sample. A small number of scattered neutrons, fulfilling the Bragg condition, are reflected by the analyzer array crystals, Si(111), and pass the sample a second time. The backscattered neutrons are collected at the detectors. The time dependence of the Doppler drive and therefore of $\delta E(t)$ is known. This allows to obtain the energy transfer ΔE of the sample.

Time-of-Flight Backscattering Instrument—IRIS. IRIS is an indirect geometry time-of-flight spectrometer located at the pulsed neutron source ISIS, Didcot, United Kingdom.[14] The incident neutron beam from the spallation source is wavelength-selected by a chopper, with a frequency of f = 50 Hz, resulting in a bandwidth of neutrons centered at λ = 6.66 Å. These neutrons scatter upon interaction with the sample in all directions and hit an analyzer array of pyrolytic graphite. Similar to EMU, those neutrons, fulfilling the Bragg condition, in this case, the (002) reflection, are reflected back from the analyzers and collected at the detectors. By knowing the total time-of-flight time, t, of the neutrons together with the distances L_1, source−sample, and L_2, sample−analyzer−detectors, the energy exchange within the sample can be determined.

Time-of-Flight Spectrometer—Pelican. Pelican is a direct time-of-flight geometry cold-neutron spectrometer at ANSTO, Sydney, Australia.[13] The incoming neutrons are monochromatized and wavelength-selected by a focusing crystal and pulsed by two Fermi choppers, which are phased in order to remove $\lambda/2$ from the neutron beam. These pulsed neutrons of λ = 6 Å scatter at the sample in all directions to be collected at the detectors. The time, t_0, needed for elastic scattering without energy transfer can be determined based on the initial energy, E_i, and the pathlength, which the neutrons need to travel until the detector is reached. The energy transfer can be determined by taking the difference in the "real" flight time, t_{tof}, which was needed including energy exchange and the elastic time, t_0. This results in the scattering intensity depending on the scattering angle and time. This instrument is able to detect larger energy transfers compared to EMU and IRIS. Thus, the simple approximation for the momentum transfer based on elastic scattering is not valid, and the law of cosines is applied.

Samples. The samples used in this study are bottlebrush polymer melts based on PDMS, i.e., PDMS-*g*-PDMS bottlebrushes. Details of the synthesis route have been previously described in a related publication.[12] These samples have been analyzed prior by dielectric spectroscopy and SANS.[12] For completeness, the resulting molecular weights, together with the polydispersity index (PDI) and the grafting density, are summarized in Table 2. A pictorial representation of the resulting shapes of the different bottlebrush polymers is illustrated in Figure 1.

Table 2. Number-Average Molecular Weight, M_n, PDI, and Grafting Density, ρ^*, of the Three Bottlebrush Samples and Their Single Component

name	single chain M_n (g/mol) (PDI)	bottlebrush M_n (kg/mol) (PDI) [ρ^*]
side chain short	298 (1.0)	95 (1.3) [89]
side chain middle	1800 (1.2)	157 (1.1) [30]
side chain long	11,500 (1.1)	1106 (1.2) [41]
backbone short	16,500 (1.1)	
backbone middle/long	13,500 (1.2)	

RESULTS

At the lowest temperatures, a weak decay with almost Q-independent relaxation times is observed in the accessible time range, as seen in Figure 3a,b. This indicates a localized motion, which at such temperatures, where the segmental dynamics are assumed to be frozen or too slow, can be attributed to the rotation of the methyl groups because all protons of the bottlebrush polymer are parts of a methyl group (Figure 2).[17]

By comparing the glass-transition temperature, determined by dielectric spectroscopy by Jakobi *et al.*[12] (Table 3), with the measurement temperature of Figure 3a,b, it reveals that these two temperatures are below T_g, thus the segmental dynamics are frozen.

With increasing temperature, the amplitude decreases slightly and the decay is still almost independent of the momentum transfer, which adds further support for the localized motions. In the long-time region, a plateau,

https://dx.doi.org/10.1021/acs.macromol.0c01846
Macromolecules 2020, 53, 9553−9562

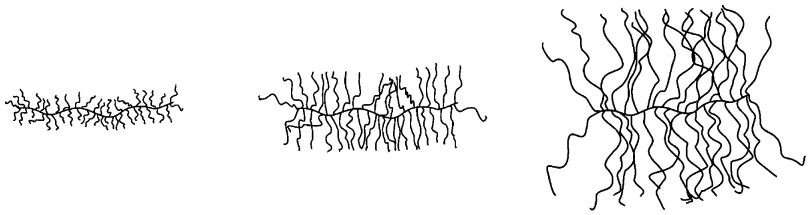

a) b) c)

Figure 1. Simplified illustration of the shape of the PDMS-*g*-PDMS bottlebrush polymers with (a) $M_n^{\text{side chain}}$ = 298 g/mol, (b) $M_n^{\text{side chain}}$ = 1800 g/mol, and (c) $M_n^{\text{side chain}}$ = 11,500 g/mol.

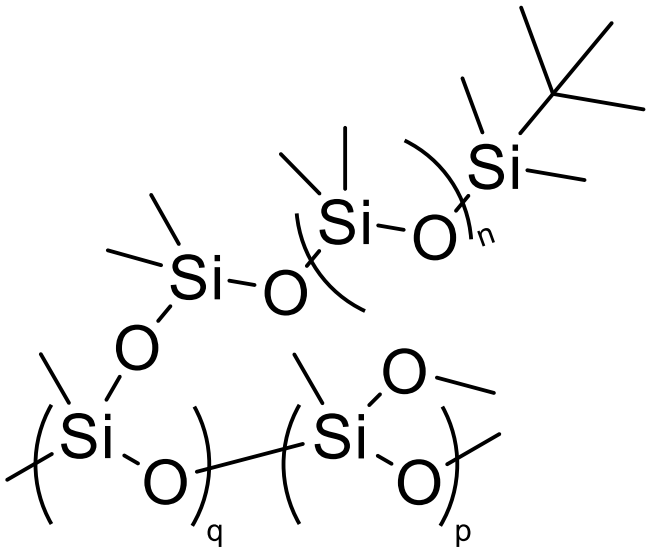

Figure 2. Chemical structure of the PDMS-*g*-PDMS bottlebrush polymer with all protons located in the methyl groups.

intensifying with increasing temperature, emerges (Figure 3c,d). Similar behavior is seen for all three samples. The data of Figure 3c,d are measured above T_g; however, based on dielectric spectroscopy data,[12] in this temperature range, the segmental dynamics are too slow to be in the available time window for QENS.

Further increasing the measurement temperature shifts the next slower dynamical process, i.e., segmental relaxation, into the available time window of QENS. Here, the methyl group dynamics are too fast to show any contributions to the intermediate scattering function, $S_{inc}(Q,t)$. In this temperature region, a full decay to 0 is visible for all Q-values in the accessible time range (Figure 4). Similar behavior is observed in all three samples (Figures S1−S4 in the Supporting Information).

Data Analysis. The experimental data suggest two different processes in the available time range, separated by temperature. Based on the results, the first process at low temperatures is identified as the methyl group rotation, whereas the second process is dominated by the segmental relaxation.

Methyl group rotations are localized and confined by their geometry, i.e., by the positions the hydrogen atoms can occupy. The mathematical framework of the so-called elastic incoherent structure factor (EISF) is very useful for describing localized motions (represented as index l), which leads to

$$S_l(Q,t) = A\cdot\exp\left(-\frac{1}{3}\langle u^2\rangle Q^2\right)\cdot \left(\text{EISF} + (1-\text{EISF})\cdot\exp\left(-\left(\frac{t}{\tau_l}\right)^{\beta_l}\right)\right) \quad (3)$$

with the Debye−Waller factor and a prefactor A. Because polymers show a distribution of different relaxation times, the Kohlrausch−Williams−Watts (KWW) function, $\exp\left(-\left(\frac{t}{\tau_l}\right)^{\beta_l}\right)$, is an appropriate way to describe the relaxation times of the involved processes.[17−20] In this context, τ_l describes the relaxation time of the methyl groups and β_l is the stretching exponent, resembling the width of the relaxation time distribution.

Typical for the EISF of the methyl group rotation is the so-called threefold jump

$$\text{EISF}(Q) = \frac{1}{3}(1 + 2j_0(QR\sqrt{3})) \quad (4)$$

with j_0 being the zeroth-order spherical Bessel function and R being the circle radius.[20−22] Here, the hydrogen atoms can jump between three equidistant positions on a circle with radius R (Figure 5a). The threefold jump, represented by the EISF, is an oscillation around EISF = 1/3 for large Q-values (Figure 5b). This assumption is also valid for our sample systems, as seen later in the data discussion.

At higher temperatures, the segmental relaxation prevails with some contributions of the Debye−Waller factor. There are no geometrical constraints imposed on the segmental relaxation; therefore, an additional EISF is not needed for the data description, and the model function is reduced to

$$S_s(Q,t) = A\cdot\exp\left(-\frac{1}{3}\langle u^2\rangle Q^2\right)\cdot\exp\left(-\left(\frac{t}{\tau_s}\right)^{\beta_s}\right) \quad (5)$$

with τ_s being the segmental relaxation time and β_s being the associated stretching parameter of the KWW function.

Both model functions have a large number of adjustable parameters. Therefore, to improve the stability of the fitting function, reasonable assumptions are needed. For the low-temperature function (eq 3), the atomistic mean-square displacement u^2 as well as the relaxation time of the localized motion τ_l and the associated stretching parameter β_l are assumed to be independent of Q. In the case of the Debye−Waller factor, the Q-dependence is already included as the Q^2 factor within the exponential function, and therefore, u^2 only depends on temperature. The relaxation time of the localized

https://dx.doi.org/10.1021/acs.macromol.0c01846
Macromolecules 2020, 53, 9553−9562

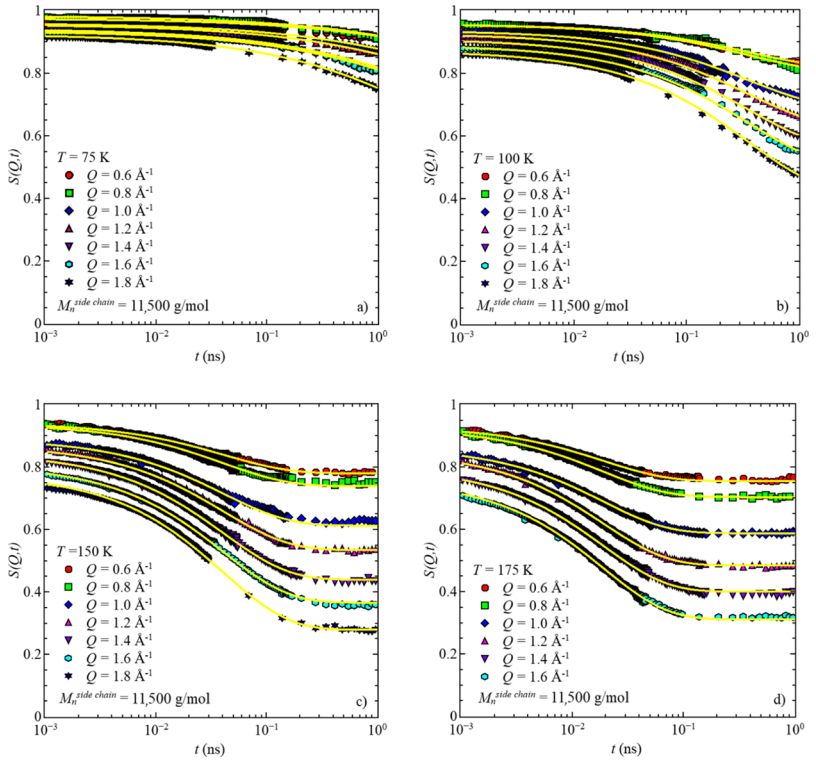

Figure 3. Intermediate scattering function, $S(Q,t)$, vs time, t, for the sample with $M_n^{\text{side chain}}$ = 11,500 g/mol for four different temperatures: (a) T = 75 K, (b) T = 100 K, (c) T = 150 K, and (d) T = 175 K. Solid lines represent the data descriptions with the model function for low temperatures, eq 3.

Table 3. Glass-Transition Temperature, T_g, of the Three Samples, Taken from the Publication of Jakobi *et al.*[12]

$M_n^{\text{side chain}}$	T_g (K)
298	140.4 ± 0.2
1800	146.2 ± 0.5
11,500	144.6 ± 0.7

motion occurs naturally on a well-restricted geometry, and therefore, no significant Q-dependence is detectable.[22] Furthermore, QENS experiments on similar sample systems have not shown any substantial dependence on Q within the experimental error for the stretching parameter, β_l.[20,23] The EISF shows an explicit Q-dependence, which is determined separately.

In the case of the segmental relaxation, described with the model function for high temperatures (eq 5), the relaxation times show a pronounced Q-dependence.[17,24,25] Therefore, τ_s needs to be determined for each Q-value independently. The stretching parameter, β_s, verified by single fits, and u^2 are treated to be independent of the momentum transfer.

All Q-values of one temperature are fitted with a so-called "Global Fit". By means of this, all Q-values are simultaneously described with the respective model function, whereby the Q-independent parameters are shared over all Q-values. Shared implies that all values do not depend on Q and should therefore be the same for all momentum transfers.

DISCUSSION

The plateau in the long-time region at the low temperatures raises the question whether the geometrical constraint of the

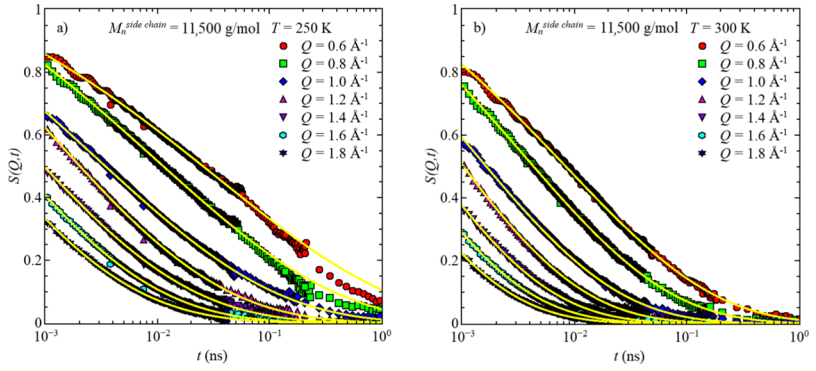

Figure 4. : Intermediate scattering function, $S(Q,t)$, vs time, t, for the sample with $M_n^{\text{side chain}}$ = 11,500 g/mol for two temperatures, (a) T = 250 K and (b) T = 300 K. Solid lines represent the data descriptions with the model function for high temperatures, eq 5.

https://dx.doi.org/10.1021/acs.macromol.0c01846
Macromolecules 2020, 53, 9553−9562

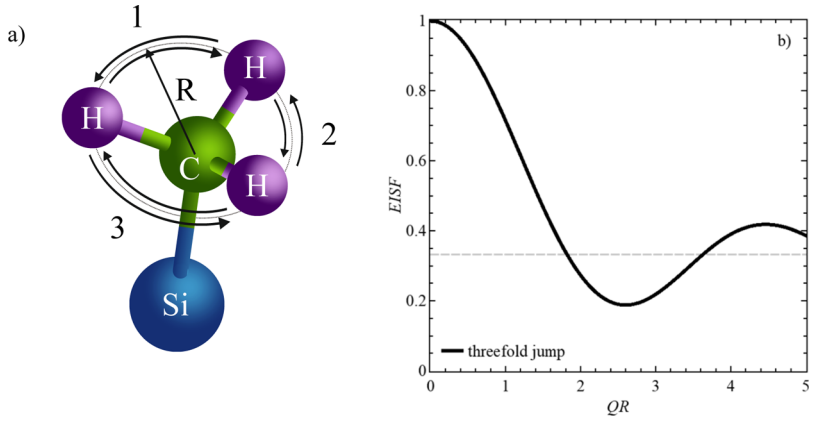

Figure 5. (a) Three-dimensional illustration of a methyl group, attached to a silicon atom, including the radius, R, of the circle spanned by the position of the hydrogen atoms. (b) EISF, vs QR of the methyl group rotation, that is, the motions of the H atoms, confined to a potential of a threefold jump.

methyl groups causes this effect. Adjusting the intermediate scattering function for the EISF and the Debye−Waller factor according to eq 6

$$S'(Q,t) = \exp\left(-\frac{t}{\tau_1}\right)^{\beta_1} = \frac{\frac{S(Q,t)}{A\cdot\exp\left(-\frac{1}{3}\cdot\langle u^2\rangle\cdot Q^2\right)} - \mathrm{EISF}}{(1-\mathrm{EISF})} \quad (6)$$

results in a full decay to 0 for all Q-values, as seen in Figure 6. This supports the assumption that the plateau is caused by the

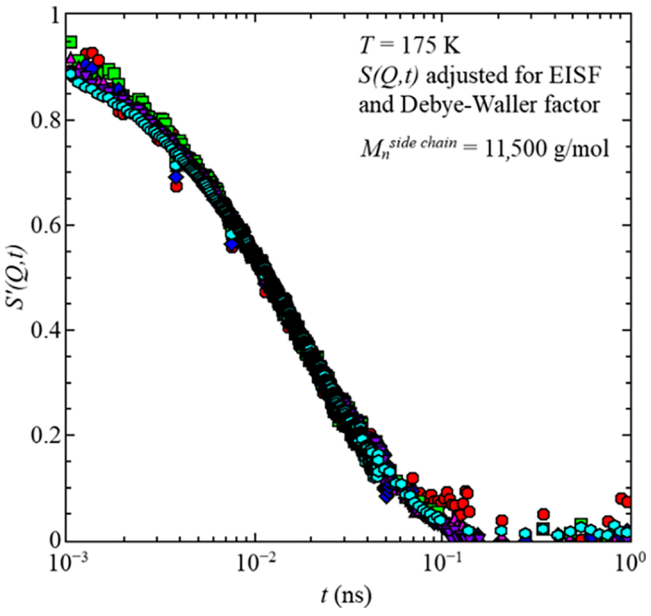

Figure 6. Adjusted intermediate scattering function, $S'(Q)$, vs time, t, for the sample with $M_n^{\text{side chain}}$ = 11,500 g/mol for all Q-values at temperature T = 175 K, cf. text.

constrained dynamics of the methyl group rotation. Similar results have been reported for poly(vinyl acetate)[26] and poly(methyl methacrylate).[20]

The resulting EISF values show a particular dependence on the temperature and the momentum transfer (Figure S5). Describing these dependencies with the classical threefold jump (eq 4), known for methyl group rotations, implies a temperature-dependent radius of the methyl group rotation, which increases by ∼28% within ΔT = 100 K and exceeds the maximum radius, that is possible based on the bond length. Therefore, a modified threefold jump model has been used including the fraction, m, of participating protons on the signal in the available time window.[20,27,28]

$$\mathrm{EISF}(Q) = (1-m) + m\cdot\left[\frac{1}{3} + \frac{2}{3}j_0(QR\sqrt{3})\right] \quad (7)$$

Here, a temperature-independent radius, R, of the methyl group rotation has been calculated based on the H−H distance of 1.79 Å,[29] resulting in R = 1.033 Å. As seen in the inset of Figure 7, the number of protons contributing to the measurement signal increases with increasing temperature and reaches 100% for the highest temperatures. This approach has previously also been applied to poly(methyl methacrylate) studies.[30] Interestingly, a nonsystematic change of the

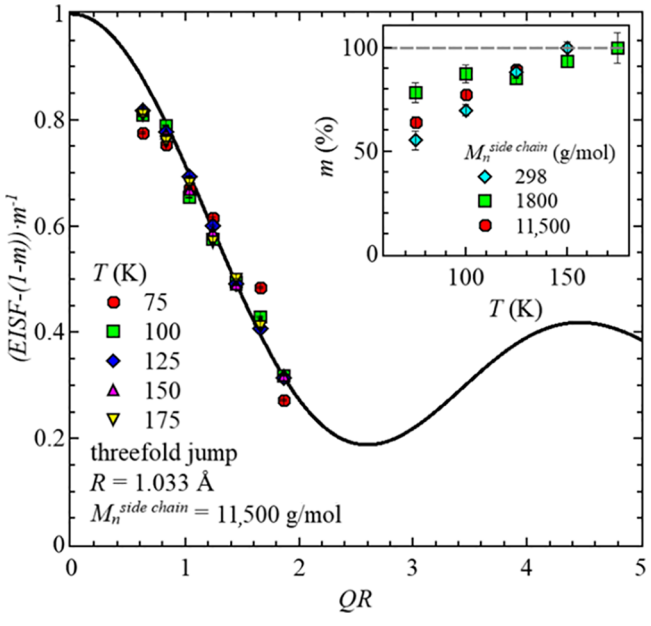

Figure 7. EISF, adjusted for the participation protons vs QR for the sample with $M_n^{\text{side chain}}$ = 11,500 g/mol at different temperatures. The solid black line represents the motion of a hydrogen atom, confined to the potential of a threefold jump. Inset: Fraction of participating protons, m, vs temperature, T, for all three samples.

https://dx.doi.org/10.1021/acs.macromol.0c01846
Macromolecules 2020, 53, 9553−9562

participating fraction depending on the molecular weight of the side chains is visible, especially at low temperatures. This could be due to the differences in the grafting density; however, a more detailed study would be needed to verify this in detail.

After adjusting the EISF for the temperature dependence of the participating proton fraction, m, all values obtained for the different temperatures superimpose, as seen in Figure 7. Here, the data can be well described with the threefold jump model, which agrees with the results in the literature of methyl group dynamics.[21,31]

The resulting stretching parameter, β_l, for all three samples, which is associated with the relaxation time distribution, shows a weak temperature dependence, as illustrated in Figure S6 in the Supporting Information. With increasing temperature, β_l increases and tends to saturate at high temperatures,[20] for the two bottlebrush polymers having $M_n^{\text{side chain}}$ = 1800 g/mol and $M_n^{\text{side chain}}$ = 11,500 g/mol. A potential consequence could be narrowing of the relaxation time distribution as the temperature increases. It could be connected to the fraction of protons contributing to the signal. In the case of the $M_n^{\text{side chain}}$ = 298 g/mol sample, the β_l parameter peaks and does not show a clear connection with the fraction of participating protons. At high temperatures, the motions of almost all protons, which are mainly located in the methyl groups, are within the available time window. Therefore, the relaxation times are more uniform and less distributed, resulting in higher β_l values. Because of the different final values, which β_l of these two samples approximates, the grafting density could have some influence on the final distribution width in the high-temperature region. However, at this point, a more detailed statement is not possible.

Focusing on the temperature dependence of the relaxation times for the localized motions, τ_l, a similar behavior is seen for all three samples. With increasing temperature, the relaxation time decreases, i.e., the relaxation speeds up (Figure 8).

This behavior follows an Arrhenius law, which implies a thermally activated process with a characteristic activation energy, E_A, describing the energy barrier the methyl group needs to overcome to perform the threefold jump, that is, a rotation around the Si−C bond to the next possible hydrogen position. The resulting fit parameters of the Arrhenius law are summarized in Table 4. For all three samples, the values are on the same orders of magnitude. Furthermore, literature values of QENS experiments on linear PDMS of E_A = (4.5 ± 0.5) kJ/mol[18,19] or E_A = 5.2 kJ/mol[32] imply that the methyl group dynamics only slightly depend on the molecular weight. However, comparing the linear and bottlebrush architectures shows significantly different activation energies, as seen in Table 4. As observed for numerous polymers, CH_3 rotations depend on the local environment.[20,22,33] According to Jakobi *et al.*,[12] the monomer density is higher closer to the backbone based on the radial monomer density distribution function deducted from the form factor description of the SANS data. Therefore, the environment along the side chains could be assumed to change. This leads to more confined CH_3 groups closer to the backbone and CH_3 groups more equivalent to linear PDMS at the outer positions of the side chains, resulting in higher activation energies on average.

Concentrating on the different side-chain lengths, slight differences occur, which could be attributed to the different grafting densities, influencing the number of different methyl groups.

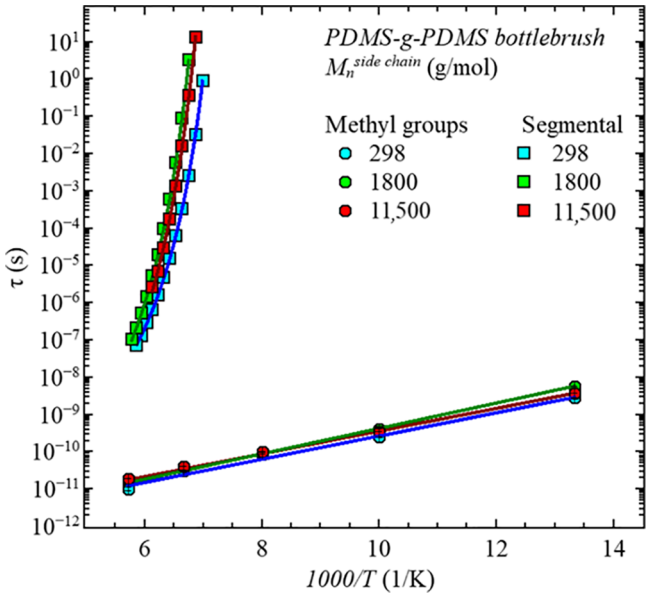

Figure 8. Relaxation times, τ, vs 1000/T of all three samples for the two relaxation processes. Round symbols refer to the methyl group dynamics measured by QENS, described by the Arrhenius law, and squared symbols refer to the segmental dynamics obtained by dielectric spectroscopy and described by the Vogel−Fulcher−Tammann (VFT) law.[12]

Table 4. Parameters Obtained from Fitting the Temperature Dependence of the Relaxation Times of the Methyl Groups in Figure 8 by the Arrhenius Law, Including the Molecular Weights of the Side Chains, $M_n^{\text{side chain}}$, the Relaxation Time for Infinitely High Temperatures, τ_∞, and the Activation Energy, E_A

$M_n^{\text{side chain}}$ (g/mol)	τ_∞ (s)	E_A (kJ/mol)
298	(2.04 ± 0.72) × 10^{-13}	6.0 ± 0.3
1800	(1.67 ± 0.11) × 10^{-13}	6.5 ± 0.1
11,500	(3.21 ± 0.22) × 10^{-13}	5.8 ± 0.1

The obtained segmental relaxation times, τ_s, from the high temperatures, show a particular Q-dependence, which follows a power law, with the slope parameter s, as seen in Figure 9.

$$\tau_s \propto Q^{-s} \tag{8}$$

While the relaxation becomes faster with increasing momentum transfer, increasing the side-chain length slows down the segmental relaxation times. Also, a temperature effect is visible. Increasing the temperature, by ΔT = 50 K, accelerates the relaxation by around half a decade. This behavior exists for each sample. The resulting power laws associated with each temperature and sample are summarized in Table 5.

For both temperatures, a pronounced decrease of the slope with increasing side-chain length is observed, as indicated by the s parameter. Here, a stronger dependence is seen for the shortest side chains at both temperatures. With increasing temperatures, s reduces, thus the Q-dependence of the relaxation time on the momentum transfer is reduced.

The stretching parameter, β_s, associated with the segmental dynamics increases slightly with temperature and molecular weight of the side chains, as seen in the inset of Figure 10. Here, the highest values are obtained for the bottlebrush polymer with $M_n^{\text{side chain}}$ = 11,500 g/mol. For linear polymers, β_s

https://dx.doi.org/10.1021/acs.macromol.0c01846
Macromolecules 2020, 53, 9553−9562

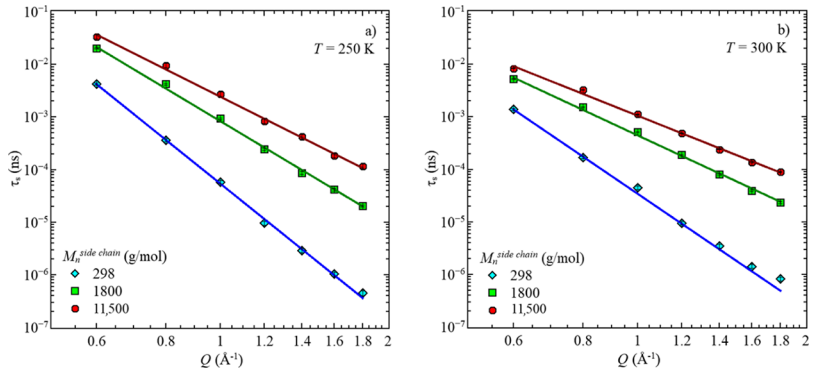

Figure 9. Segmental relaxation time, τ_s, vs momentum transfer, Q, of all three samples for two temperatures, (a) T = 250 K and (b) T = 300 K. Solid lines are the power law description with eq 8.

Table 5. Parameters Obtained from the Power Law Description of the Segmental Relaxation Times, τ_s, as a Function of Momentum Transfer, Q, in Figure 9, Including the Number-Average Molecular Weight of the Side Chains, $M_n^{\text{side chain}}$, and the Slope Parameters, s, for the Two Temperatures, T = 250 K and T = 300 K

$M_n^{\text{side chain}}$	s (T = 250 K)	s (T = 250 K)
298	(8.52 ± 0.02)	(7.24 ± 0.09)
1800	(6.35 ± 0.13)	(4.96 ± 0.12)
11,500	(5.31 ± 0.12)	(4.24 ± 0.10)

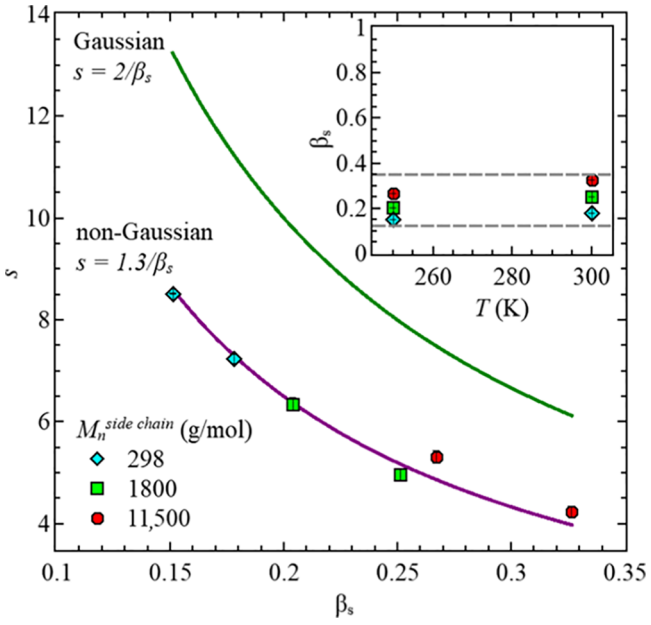

Figure 10. Slope parameter, s, vs stretching parameter, β_s, for all three PDMS-g-PDMS bottlebrush polymers. Inset: stretching parameter, β_s, vs temperature, T, for all three samples.

= 0.4−0.6 is reported.[17,34] Our values are continually below β_s = 0.4 for all side-chain lengths, i.e., our relaxation time distribution is broader compared to that of linear polymers. Because with increasing $M_n^{\text{side chain}}$, the values increase, it could be assumed that the low β_s values are routed in the bottlebrush architecture and may reach values known for linear polymers with sufficiently long side chains. This is in agreement with recent findings of dielectric spectroscopy.[12] Here, a reduction of segmental relaxation times was found, by comparing those from linear side chains to the grafted side chains. The strongest reduction was reported for the shortest side chains and almost identical relaxation times for the longest side-chain length. This could suggest different relaxation times within the side chains of the bottlebrush polymers, i.e., a distribution of relaxation times. Furthermore, it could be interpreted in a way that the inner segments are influenced the most, and with increasing side-chain length, this effect saturates and finally, relaxation times approximate the relaxation times of a linear polymer. Thus, the distribution narrows with increasing side-chain length. This is also reflected in the stretching parameter β_s. The longer the side chain length, the larger and more similar the β_s values are to those of linear polymers. Therefore, the relaxation times show a narrower distribution for longer side-chain lengths.

In general, the shape parameter, s, can be related to the stretching parameter, β_s, which allows to clarify the underlying behavior of the system. For systems showing a Gaussian behavior, this relationship can be described by $s = 2/\beta_s$.[17,35] Using this relationship results in the solid green line in Figure 10. The fit values, β_s (filled symbols), for our PDMS-g-PDMS bottlebrush polymers are different, hence not confirming Gaussian behavior. However, the relationship of s and β_s can be well described with $s = 1.3/\beta_s$, as shown with the solid purple line in Figure 10. Based on this, we suggest a non-Gaussian behavior for all our three samples in the available Q-range, which is equivalent to a heterogeneous system. Similar descriptions have been reported for polybutadiene, $s = 1.4/\beta_s$, and for polyisoprene, $s = 1.3/\beta_s$.[31,36]

To verify that the segmental relaxation, obtained by QENS, belongs to the α-relaxation, as determined by dielectric spectroscopy, a comparison of the relaxation times obtained from both techniques is very common.[17,37,38] The relaxation times obtained by dielectric spectroscopy together with τ_s for every Q-value are shown in Figure 11 for all three samples. Here, the same behavior as reported by dielectric spectroscopy is seen in the data obtained by QENS. With increasing temperature, the relaxation times decreases.

SUMMARY AND CONCLUSIONS

We have used QENS to follow the short-time dynamics on PDMS-g-PDMS bottlebrush polymers. Three different samples have been used, having different side-chain lengths, while the backbone length is similar. SANS revealed a shape transition from ellipsoidal toward an elongated shape, with decreasing side-chain length.[12] In order to cover a broad time range for dynamical studies, a combination of three different neutron

https://dx.doi.org/10.1021/acs.macromol.0c01846
Macromolecules 2020, 53, 9553−9562

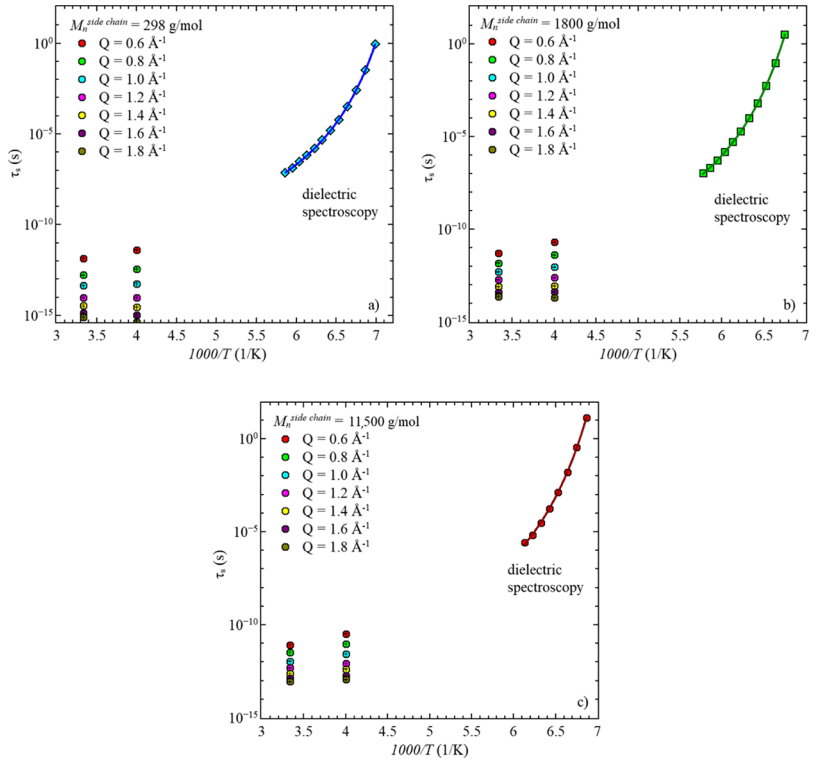

Figure 11. Segmental relaxation times, τ_s, vs $1000/T$ of the three samples with different side-chain lengths, obtained by dielectric spectroscopy and QENS. (a) $M_n^{side\ chain}$ = 298 g/mol, (b) $M_n^{side\ chain}$ = 1800 g/mol, and (c) $M_n^{side\ chain}$ = 11,500 g/mol. Solid lines in the low-temperature region are data descriptions of the dielectric spectroscopy data by the VFT equation.

spectrometer instruments was used, resulting in a time range from 1 ps to 1 ns. This time window includes two processes: localized motions at low temperatures and segmental dynamics at higher temperatures. The localized motions have been identified as methyl group rotations, which are confined by their geometry and can be described by a threefold jump model considering the participating fraction of the protons in the available time window. While the relaxation time of this dynamical process is independent of the side-chain length and the momentum transfer, the segmental relaxation times show a well-pronounced dependence on both the molecular weight of the side chains and the momentum transfer. Here, the relaxation time decreases with increasing momentum transfer and decreasing side-chain length. The Q-dependence of the segmental relaxation times follows a power law, resulting in the slope parameter s. Based on this parameter, a relationship to the stretching parameter, β_s, can be established, suggesting a non-Gaussian behavior for our PDMS-g-PDMS bottlebrush polymers.

■ ASSOCIATED CONTENT

Supporting Information

The Supporting Information is available free of charge at https://pubs.acs.org/doi/10.1021/acs.macromol.0c01846.

Time-dependent intermediate scattering functions for the samples with $M_n^{side\ chain}$ = 298 g/mol and $M_n^{side\ chain}$ = 1800 g/mol; Q-dependence of the EISF for the sample with $M_n^{side\ chain}$ = 11,500 g/mol for selected temperatures; and stretching parameter, β_l, as a function of temperature, T, of the methyl group dynamics for all three PDMS-g-PDMS bottlebrush samples (PDF)

■ AUTHOR INFORMATION

Corresponding Authors

Karin J. Bichler − *Department of Physics &Astronomy, Louisiana State University, Baton Rouge 70803, Louisiana, United States;* orcid.org/0000-0002-8666-1859; Email: kbichler@lsu.edu

Gerald J. Schneider − *Department of Physics &Astronomy and Department of Chemistry, Louisiana State University, Baton Rouge 70803, Louisiana, United States;* orcid.org/0000-0002-5577-9328; Email: gjschneider@lsu.edu

Authors

Bruno Jakobi − *Department of Chemistry, Louisiana State University, Baton Rouge 70803, Louisiana, United States;* orcid.org/0000-0003-1171-9486

Victoria García Sakai − *ISIS Facility, Rutherford Appleton Laboratory, Didcot OX11 0QX, U.K.*

Alice Klapproth − *Australian Nuclear Science and Technology Organisation, Lucas Heights 2234, New South Wales, Australia*

Richard A. Mole − *Australian Nuclear Science and Technology Organisation, Lucas Heights 2234, New South Wales, Australia;* orcid.org/0000-0001-5018-4221

Complete contact information is available at: https://pubs.acs.org/10.1021/acs.macromol.0c01846

Notes

The authors declare no competing financial interest.

■ ACKNOWLEDGMENTS

We acknowledge funding by the U.S. Department of Energy (DoE) under grant DE-SC0019050. We are also grateful for the access to the neutron scattering instruments, provided by

ACNS, Sydney, Australia (P7387 and P7389) and the ISIS Neutron and Muon Facility (DOI: 10.5286/ISIS.E.RB1910220).

REFERENCES

(1) Pesek, S. L.; Li, X.; Hammouda, B.; Hong, K.; Verduzco, R. Small-Angle Neutron Scattering Analysis of Bottlebrush Polymers Prepared via Grafting-through Polymerization. *Macromolecules* **2013**, *46*, 6998−7005.

(2) Verduzco, R.; Li, X.; Pesek, S. L.; Stein, G. E. Structure, Function, Self-Assembly, and Applications of Bottlebrush Copolymers. *Chem. Soc. Rev.* **2015**, *44*, 2405−2420.

(3) Bichler, K. J.; Jakobi, B.; Huber, S. O.; Gilbert, E. P.; Schneider, G. J. Structural Analysis of Ultrasoft PDMS-g-PDMS Shell-Only Particles. *Macromolecules* **2020**, *53*, 78−89.

(4) Rathgeber, S.; Pakula, T.; Wilk, A.; Matyjaszewski, K.; Beers, K. L. On the Shape of Bottle-Brush Macromolecules: Systematic Variation of Architectural Parameters. *J. Chem. Phys.* **2005**, *122*, 124904.

(5) Dutta, S.; Wade, M. A.; Walsh, D. J.; Guironnet, D.; Rogers, S. A.; Sing, C. E. Dilute Solution Structure of Bottlebrush Polymers. *Soft Matter* **2019**, *15*, 2928−2941.

(6) Bolisetty, S.; Rosenfeldt, S.; Rochette, C. N.; Harnau, L.; Lindner, P.; Xu, Y.; Müller, A. H. E.; Ballauff, M. Interaction of Cylindrical Polymer Brushes in Dilute and Semi-Dilute Solution. *Colloid Polym. Sci.* **2009**, *287*, 129−138.

(7) Levi, A. E.; Lequieu, J.; Horne, J. D.; Bates, M. W.; Ren, J. M.; Delaney, K. T.; Fredrickson, G. H.; Bates, C. M. Miktoarm Stars via Grafting-through Copolymerization: Self-Assembly and the Star-to-Bottlebrush Transition. *Macromolecules* **2019**, *52*, 1794−1802.

(8) Daniel, W. F. M.; Burdyńska, J.; Vatankhah-Varnoosfaderani, M.; Matyjaszewski, K.; Paturej, J.; Rubinstein, M.; Dobrynin, A. V.; Sheiko, S. S. Solvent-Free, Supersoft and Superelastic Bottlebrush Melts and Networks. *Nat. Mater.* **2016**, *15*, 183−189.

(9) Pesek, S. L.; Lin, Y.-H.; Mah, H. Z.; Kasper, W.; Chen, B.; Rohde, B. J.; Robertson, M. L.; Stein, G. E.; Verduzco, R. Synthesis of Bottlebrush Copolymers Based on Poly(dimethylsiloxane) for Surface Active Additives. *Polymer* **2016**, *98*, 495−504.

(10) McLeish, T. C. B.; Milner, S. T. Entangled Dynamics and Melt Flow of Branched Polymers. *Branched Polymers Ii*; Springer, 1999; pp 195−256.

(11) López-Barrón, C. R.; Brant, P.; Eberle, A. P. R.; Crowther, D. J. Linear Rheology and Structure of Molecular Bottlebrushes with Short Side Chains. *J. Rheol.* **2015**, *59*, 865−883.

(12) Jakobi, B.; Bichler, K. J.; Sokolova, A.; Schneider, G. J. Dynamics of PDMS-g-PDMS Bottlebrush Polymers by Broadband Dielectric Spectroscopy. *Macromolecules* **2020**, *53* (19), 8450−8458.

(13) Yu, D.; Mole, R.; Noakes, T.; Kennedy, S.; Robinson, R. Pelican — a Time of Flight Cold Neutron Polarization Analysis Spectrometer at OPAL. *J. Phys. Soc. Jpn.* **2013**, *82*, SA027.

(14) Demmel, F.; McPhail, D.; French, C.; Maxwell, D.; Harrison, S.; Boxall, J.; Rhodes, N.; Mukhopadhyay, S.; Silverwood, I.; Sakai, V. G.; Fernandez-Alonso, F. Tof-Backscattering Spectroscopy at the ISIS Facility: Status and Perspectives. *J. Phys.: Conf. Ser.* **2018**, *1021*, 012027.

(15) de Souza, N. R.; Klapproth, A.; Iles, G. N. EMU: High-Resolution Backscattering Spectrometer at ANSTO. *J. Neutron Res.* **2016**, *27*, 20−21.

(16) Arnold, O.; Bilheux, J. C.; Borreguero, J. M.; Buts, A.; Campbell, S. I.; Chapon, L.; Doucet, M.; Draper, N.; Ferraz Leal, R.; Gigg, M. A.; Lynch, V. E.; Markvardsen, A.; Mikkelson, D. J.; Mikkelson, R. L.; Miller, R.; Palmen, K.; Parker, P.; Passos, G.; Perring, T. G.; Peterson, P. F.; Ren, S.; Reuter, M. A.; Savici, A. T.; Taylor, J. W.; Taylor, R. J.; Tolchenov, R.; Zhou, W.; Zikovsky, J. Mantid—Data Analysis and Visualization Package for Neutron Scattering and μ SR Experiments. *Nucl. Instrum. Methods Phys. Res., Sect. A* **2014**, *764*, 156−166.

(17) Gerstl, C.; Schneider, G. J.; Fuxman, A.; Zamponi, M.; Frick, B.; Seydel, T.; Koza, M.; Genix, A.-C.; Allgaier, J.; Richter, D.; Colmenero, J.; Arbe, A. Quasielastic Neutron Scattering Study on the Dynamics of Poly(alkylene oxide)s. *Macromolecules* **2012**, *45*, 4394−4405.

(18) Arrighi, V.; Ganazzoli, F.; Zhang, C.; Gagliardi, S. New Interpretation of Local Dynamics of Poly (dimethyl siloxane) Observed by Quasielastic Neutron Scattering. *Phys. Rev. Lett.* **2003**, *90*, 058301.

(19) Arrighi, V.; Gagliardi, S.; Zhang, C.; Ganazzoli, F.; Higgins, J. S.; Ocone, R.; Telling, M. T. F. A Unified Picture of the Local Dynamics of Poly(dimethylsiloxane) across the Melting Point. *Macromolecules* **2003**, *36*, 8738−8748.

(20) Arrighi, V.; Higgins, J. S.; Burgess, A. N.; Howells, W. S. Rotation of Methyl Side Groups in Polymers: A Fourier Transform Approach to Quasielastic Neutron Scattering. 1. Homopolymers. *Macromolecules* **1995**, *28*, 2745−2753.

(21) Zorn, R.; Frick, B.; Fetters, L. J. Quasielastic Neutron Scattering Study of the Methyl Group Dynamics in Polyisoprene. *J. Chem. Phys.* **2002**, *116*, 845−853.

(22) Arrighi, V.; Higgins, J. S. Side Group Rotations in Amorphous Polymers. *Phys. B* **1996**, *226*, 1−9.

(23) Gerstl, C. *Kettenkonformation und Dynamik verschiedener Poly(alkylenoxid)e*; Westfälische Wilhlems-Universität Münster, 2011.

(24) Colmenero, J.; Arbe, A. A.; Alegría, A.; Ngai, K. L. Q-Dependence of the Relaxation Times of the α-Relaxation as Observed by Quasielastic Neutron Scattering. *J. Non-Cryst. Solids* **1994**, *172*−*174*, 229−233.

(25) Colmenero, J. Segmental Dynamics in Polymer Melts by Relaxation Techniques and Quasielastic Neutron Scattering. *Phys. Scr.* **1993**, *T49A*, 227−232.

(26) Zhang, C.; Arrighi, V.; Gagliardi, S.; McEwen, I. J.; Tanchawanich, J.; Telling, M. T. F.; Zanotti, J.-M. Quasielastic Neutron Scattering Measurements of Fast Process and Methyl Group Dynamics in Glassy Poly(vinyl acetate). *Chem. Phys.* **2006**, *328*, 53−63.

(27) Jalarvo, N.; Tyagi, M.; Crawford, M. K. *Quasielastic Neutron Scattering Study of Poss Ligand Dynamics, EPJ Web of Conferences*; EDP Sciences, 2015; p 02007.

(28) Zorn, R.; Arbe, A.; Colmenero, J.; Frick, B.; Richter, D.; Buchenau, U. Neutron Scattering Study of the Picosecond Dynamics of Polybutadiene and Polyisoprene. *Phys. Rev. E: Stat. Phys., Plasmas, Fluids, Relat. Interdiscip. Top.* **1995**, *52*, 781−795.

(29) Amaral, L. Q.; Vinhas, L. A.; Herdade, S. B. *Neutron Transmission Study of the Rotacional Freedom of Methyl Groups in Polydimethylsiloxane*; Brazil, 1973; p 19.

(30) Arrighi, V.; Higgins, J. S.; Burgess, A. N.; Howells, W. S. Rotation of Methyl Side Groups in Polymers: A Fourier Transform Approach to Quasielastic Neutron Scattering. 2. Polymer Blends. *Macromolecules* **1995**, *28*, 4622−4630.

(31) Zorn, R.; Arbe, A.; Colmenero, J.; Frick, B.; Richter, D.; Buchenau, U. Neutron Scattering Study of the Picosecond Dynamics of Polybutadiene and Polyisoprene. *Phys. Rev. E: Stat. Phys., Plasmas, Fluids, Relat. Interdiscip. Top.* **1995**, *52*, 781.

(32) Grapengeter, H.-H.; Alefeld, B.; Kosfeld, R. An Investigation of Micro-Brownian Motions in Polydimethylsiloxane by Complementary Incoherent-Neutron-Scattering and Nuclear-Magnetic-Resonance Experiments Below Room Temperature. *Colloid Polym. Sci.* **1987**, *265*, 226−233.

(33) Frick, B.; Fetters, L. J. Methyl Group Dynamics in Glassy Polyisoprene: A Neutron Backscattering Investigation. *Macromolecules* **1994**, *27*, 974−980.

(34) Richter, D.; Monkenbusch, M.; Arbe, A.; Colmenero, J. *Neutron Spin Echo in Polymer Systems*; Springer-Verlag Berlin Heidelberg: Berlin, Heidelberg, 2005; p IX-246.

(35) Tyagi, M.; Alegría, A.; Colmenero, J. Heterogeneous Dynamics of Poly(vinyl acetate) far above T_g: A Combined Study by Dielectric Spectroscopy and Quasielastic Neutron Scattering. *J. Chem. Phys.* **2005**, *122*, 244909.

https://dx.doi.org/10.1021/acs.macromol.0c01846
Macromolecules 2020, 53, 9553−9562

(36) Zorn, R. Deviation from Gaussian Behavior in the Self-Correlation Function of the Proton Motion in Polybutadiene. *Phys. Rev. B: Condens. Matter Mater. Phys.* **1997**, *55*, 6249.
(37) Schönhals, A.; Kremer, F. Amorphous Polymers. *Polym. Sci.: Compr. Ref.* **2012**, *1*, 201−226.
(38) Gambino, T.; Alegría, A.; Arbe, A.; Colmenero, J.; Malicki, N.; Dronet, S.; Schnell, B.; Lohstroh, W.; Nemkovski, K. Applying Polymer Blend Dynamics Concepts to a Simplified Industrial System. A Combined Effort by Dielectric Spectroscopy and Neutron Scattering. *Macromolecules* **2018**, *51*, 6692−6706.

https://dx.doi.org/10.1021/acs.macromol.0c01846
Macromolecules 2020, 53, 9553−9562